Dyes and Pigments 107 (2014) 146–152

Contents lists available at ScienceDirect

Dyes and Pigments

journal homepage: www.elsevier.com/locate/dyepig

A novel near-infrared-emitting cyclometalated platinum (II) complex with donor–acceptor–acceptor chromophores

Junting Yu [a], Keqi He [a], Yanhu Li [b], Hua Tan [a], Meixiang Zhu [a], Yafei Wang [a], Yu Liu [a], Weiguo Zhu [a,*], Hongbin Wu [b,*]

[a] College of Chemistry, Key Lab of Environment-Friendly Chemistry and Application in the Ministry of Education, Xiangtan University, Xiangtan 411105, PR China

[b] Institute of Polymer Optoelectronic Materials and Devices, South China University of Technology, Guangzhou 510640, PR China

ARTICLE INFO

Article history:
Received 28 January 2014
Received in revised form
22 March 2014
Accepted 29 March 2014
Available online 5 April 2014

Keywords:
Donor–acceptor–acceptor
Platinum (II) complexes
Near-infrared emission
Electrophosphorescence
Polymer light-emitting devices
Synthesis

ABSTRACT

A novel near-infrared-emitting cyclometalated platinum (II) complex of (TPA-BT-Q)Ptpic with a donor–acceptor–acceptor (D–A–A) chromophores was synthesized and characterized, in which the TPA-BT-Q unit is a cyclometalated ligand of N,N-di(4-octyloxyphenyl)-4-(7-(quinolin-2-yl)-benzo[c][1,2,5]thiadiazol-4-yl)-phenylamine and pic is picolinate anion. Its optophysical, electrochemical and electroluminescent characteristics were primarily studied. An intense UV–vis absorption peak at 540 nm and a strong near-infrared emission peak at 759 nm were observed for (TPA-BT-Q)Ptpic in dichloromethane. Using (TPA-BT-Q)Ptpic as a single dopant and a blend of poly(vinylcarbazole) and 2-tert-butylphenyl-5-biphenyl-1,3,4-oxadiazole as a host matrix, the single-emissive-layer polymer light-emitting devices exhibited a near-infrared emission peaked at 760 nm with the maximum external quantum efficiency of 0.12% at 16.6 mA cm^{-2} and a radiance intensity of 112 μW cm^{-2} at 11.7 mA cm^{-2} at the doping concentrations of 2.0 wt%. This work provides an efficient approach to realize near-infrared electrophosphorescent emission with high radiance intensity by employing platinum (II) complex with the D–A–A structure.

© 2014 Elsevier Ltd. All rights reserved.

1. Introduction

Recently, the research on near-infrared (NIR) organic luminescent materials has gained great attentions due to their diverse potential applications in night-vision displays, sensors, optical communication, and offering superior biocompatibility for medical systems [1]. The developed NIR-emitting materials mostly contain lanthanide complexes [2], fluorescent materials with a donor–acceptor (D–A) structure [3], boron dipyrromethene dyes [4] and transition-metal complexes [5]. Among these materials, transition-metal complexes are available to exhibit higher emission efficiency due to their strong spin-orbit coupling in the presence of heavy metals, which leads to an internal quantum efficiency as high as 100% [6]. Metalloporphyrin is the most typical class in the reported transition-metal complexes and has recorded an external quantum efficiency (EQE) maximum of 2.49% for polymer light-emitting devices (PLEDs) and 9.2% for organic light-emitting devices (OLEDs) with NIR emission in the 760–780 nm range. However, these EQE levels were typically obtained at very low current densities [7]. It is well known that squareplanar platinum (II) complexes have rapidly developed in OLEDs with high-efficiency red, green, blue and even white emission by tuning their molecular structures [8]. But, few platinum (II) complexes besides Pt-porphyrin complexes have displayed satisfactory EQE level in NIR emission. In order to develop new NIR-emitting platinum (II) complexes, Gao et al. reported a platinum complex of ppyPtq, which displayed an EL emission peaked at 730 nm without EQE datum [5b]. Che et al. reported a series of neutral platinum complexes containing substituted 8-hydroxyquinoline, which gave a deep-red emission peak from 650 to 695 nm with another weak NIR emission peak from 705 to 755 nm in the device with an EQE of 1.7% [5e]. Recently, some NIR-emitting organic and polymeric fluorescent materials with donor (D) and acceptor (A) chromophores were developed because the band gap levels and photoelectronic properties can be readily tuned through a systematic variation between the D and A units [1,9]. For example, Wang et al. reported a class of fluorescent materials with D–π–A–π–D type chromophore,

* Corresponding authors. Tel.: +86 731 58298280; fax: +86 731 58292251.
E-mail addresses: zhuwg18@126.com (W. Zhu), hbwu@scut.edu.cn (H. Wu).

http://dx.doi.org/10.1016/j.dyepig.2014.03.040
0143-7208/© 2014 Elsevier Ltd. All rights reserved.

which displayed emission exclusively at 1080 nm with an EQE of 0.28% in the OLEDs [10]. Reynolds et al. reported a family of conjugated oligomers with a multi-heterocycle D–A–D structure, which displayed emission ranging from 651 to 1088 nm with an EQE of 0.87% in the PLEDs [3a].

As phosphorescent materials have exhibited higher external quantum efficiency than fluorescent materials in OLEDs, it was always interesting in developing NIR-emitting platinum complexes. In order to study effect of molecular structure of platinum complexes on NIR-emitting property, a type of platinum complexes of (Piq-G)Pt(acac) with D–A chromophores was obtained in our previous work, which exhibited an emission with a peak at 640 nm and a shoulder at 700 nm [11]. There was about 40–60 nm red-shift compared to that from the non-functionalized platinum (II) complex of (Piq)Pt(acac). Based on this findings, we here designed another novel platinum (II) complex of (TPA-BT-Q)Ptpic with D–A–A type chromophores, in which a triphenylamine (TPA) was used as an electron donor unit, a benzothiadiazole (BT) and a quinoline (Q) were simultaneously employed as strong electron acceptor units. In this (TPA-BT-Q)Ptpic, the non-planar TPA unit is available to improve carrier-transporting properties and suppress aggregations, the BT unit is a good class of luminescence units in OLEDs and acceptor units in organic solar cells (OSCs) reported in recent years [12], two alkoxy groups are benefit to improve solubility. Therefore, the (TPA-BT-Q)Ptpic with D–A–A units should provide low-energy near-infrared emission more easily than those counterparts with D–A units. The synthetic route of (TPA-BT-Q)Ptpic is shown in Scheme 1. For comparison, the counterpart of PQPtpic was made. Using (TPA-BT-Q)Ptpic as a single dopant and a blend of poly(vinylcarbazole) (PVK) and 2-*tert*-butylphenyl-5-biphenyl-1,3,4-oxadiazole (PBD) as the host matrix, we fabricated the single-emissive-layer (SEL) PLEDs by solution process and studied the device performances. A NIR emission peaked at 760 nm with a maximum EQE of 0.12% at 16.6 mA cm^{-2} and an irradiance intensity of 112 μW cm^{-2} (obtained at an applied current density of 11.7 mA cm^{-2}) were observed in the device at 2.0 wt% dopant concentration. This work indicates that introducing D–A–A structure is an efficient approach to constructure NIR-emitting platinum (II) complex and obtained high-efficiency NIR-emitting PLEDs with high radiance intensity.

2. Experimental

2.1. General information

The solvents were carefully dried and distilled by standard procedures before use. All chemicals, unless otherwise stated were obtained from commercial sources and used as received. The Suzuki coupling and cyclometalated reactions were carried out in inert gas atmosphere and monitored by thin-layer chromatography (TLC). ^{1}H NMR spectra was recorded with a Bruker Dex-400 NMR instrument using $CDCl_3$ as a solvent. Elemental analysis was carried out with a Harrios elemental analysis instrument. Mass spectrum was recorded on a Voyager Depro MALDI-TOF spectrometer. UV–vis absorption and photoluminescent spectra were recorded with a Shimadzu UV-265 spectrophotometer and a Perkin–Elmer LS-50 luminescence spectrometer, respectively. Thermogravimetric analysis (TGA) was conducted under a dry nitrogen gas flow at a heating rate of 20 °C min^{-1} on a Perkin–Elmer TGA 7 instruments. Surface morphologies were recorded by AFM on a Veeco, DI

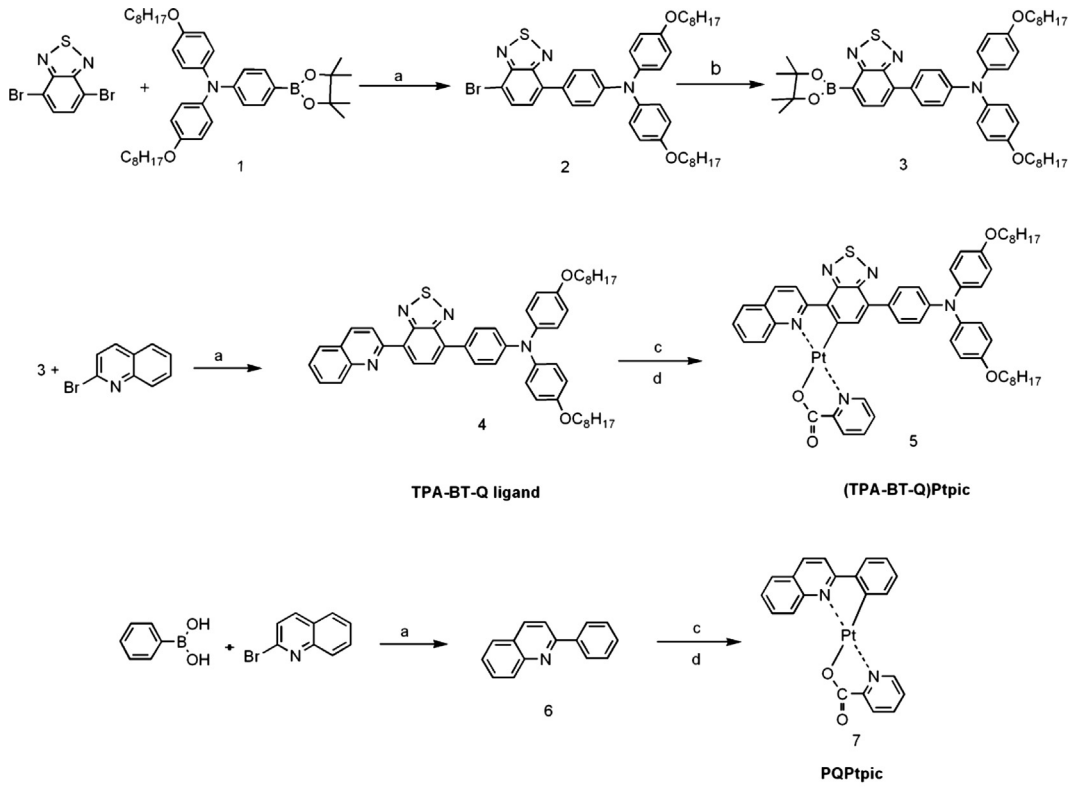

Scheme 1. Synthetic route of (TPA-BT-Q)Ptpic and PQPtpic.

Multimode NS-3D apparatus in a trapping mode under normal air condition at room temperature (RT). Cyclic voltammetry was performed on a CHI600E electrochemical work station with a scan rate of 100 mV s^{-1} at room temperature under argon, in which a Pt disk, Pt plate, and Ag/AgCl electrode were used as working electrode, counter electrode, and reference electrode in n-Bu_4NPF_6 (0.1 M) acetonitrile solution, respectively. For calibration, the redox potential of ferrocene/ferrocenium (Fc/Fc^+) was measured under the same conditions.

The cyclometalated platinum (II) complexes were also synthesized according to the literature procedures [13]. A mixture of K_2PtCl_4, CN-chelate ligand of TPA-BT-Q (or PQ) (1.2 equiv.), 2-ethoxyethanol and distilled water (3:1, *V*/*V*) was stirred under nitrogen atmosphere at 80 °C for 24 h. After cooled to RT, the precipitate was formed, then collected by filtration and washed successively with water, ethanol and hexane, respectively. The chloro-bridged dimer was obtained. This dimer was mixed with picolinic acid (2.5 equiv.) and anhydrous Na_2CO_3 (6 equiv.) in 2-ethoxyethanol. The resulting mixture was stirred under nitrogen atmosphere at 100 °C for 16 h. After cooled to RT, the resulting precipitate was collected by filtration and washed successively with water, ethanol and hexane, respectively. The residue was purified by flash chromatography on silica gel using DCM/ethyl acetate (*V*/*V* = 5/1) as eluent to provide the cyclometalated platinum (II) complexes.

2.2. PLEDs fabrication

The single-emissive-layer (SEL) PLEDs using (TPA-BT-Q)Ptpic as dopant was fabricated by spin-coating and vacuum thermal evaporation. The device configuration is ITO/PEDOT:PSS, 40 nm/PVK-30 wt% PBD:dopant, 80 nm/CsF, 1.5 nm/Al, 100 nm, where indium tin oxide (ITO) acts as the anode, poly(3,4-ethylenedioxy thiophene):poly(styrenesulfonate) (PEDOT:PSS) is used as an anode buffer layer at the interface of ITO, LiF and Al are employed as electron injection layer and cathode layer, respectively. The light-emitting layer consists of PVK, PBD and dopant, where PVK acts as the host material due to its excellent film-forming and hole-transporting properties. To facilitate electron transport in the light-emitting layer, PBD is simultaneously mixed with PVK. The weight ratio of PVK and PBD is 70:30 (*W*/*W*). The dopant concentrations vary from 0.5 wt% to 8.0 wt%. The irradiance intensity of the NIR PLEDs is measured by an integrating spheres coupled with UDT A370 spectrometer.

2.3. Syntheses

2.3.1. N,N-di(4-octyloxyphenyl)-4-(7-bromobenzo[c][1,2,5]thiadiazol-4-yl)benzenamine (**2**)

A mixture of compound **1** (1.00 g, 1.59 mmol), 4,7-dibromobenzo[c][1,2,5]thiadiazole (0.56 g, 1.91 mmol), K_2CO_3 (8 mL, 2 M) and tetrakis(triphenylphosphine) palladium (60 mg, 0.05 mmol) in toluene (50 mL) and methanol (8 mL) was heated at 80 °C under nitrogen atmosphere for 12 h. After cooled to RT, the mixture was poured into water (150 mL), extracted with DCM (3 × 30 mL). The combined organic layer was dried over $MgSO_4$ and then concentrated under reduced pressure. The residue was purified by silica gel column chromatography using DCM/petroleum ether (*V*/*V* = 1/5) as eluent to gain red viscous compound **2** (0.85 g, 60.7%). ^{1}H NMR (400 MHz, $CDCl_3$, ppm): 7.88 (d, *J* = 7.6 Hz, 1H), 7.74 (d, *J* = 8.4 Hz, 2H), 7.51 (d, *J* = 7.6 Hz, 1H), 7.13 (d, *J* = 8.6 Hz, 4H), 7.03 (d, *J* = 8.4 Hz, 2H), 6.86 (d, *J* = 8.6 Hz, 4H), 3.96–3.93 (t, *J* = 6.4 Hz, 4H), 1.85–1.75 (m, 4H), 1.45–1.26 (br, 20H), 0.89–0.88 (t, *J* = 3.2 Hz, 6H).

2.3.2. N,N-di(4-octyloxyphenyl)-4-(7-(4,4,5,5-tetramethyl-1,3,2-dioxaborolan-2-yl)benzo[c][1,2,5]thiadiazol-4-yl)benzenamine (**3**)

A mixture of compound **2** (0.60 g, 0.84 mmol), bis(pinacolato) diboron (1.71 g, 6.72 mmol), potassium acetate (0.82 g, 8.40 mmol) and Pd(dppf)Cl·CH_2Cl_2 adduct (30 mg, 0.04 mmol) in anhydrous tetrahydrofuran (50 mL) was heated at 60 °C at nitrogen atmosphere for 12 h. After cooled to RT, the mixture was poured into water (150 mL) and extracted with DCM (3 × 30 mL). The combined organic layer was dried over $MgSO_4$ and then concentrated under reduced pressure. The residue was purified by silica gel column chromatography using DCM/petroleum ether (*V*/*V* = 1/1) as eluent to gain red viscous compound **3** (0.40 g, 62.9%). ^{1}H NMR (400 MHz, $CDCl_3$, ppm): 8.26 (d, *J* = 6.8 Hz, 1H), 7.84 (d, *J* = 8.4 Hz, 2H), 7.72 (d, *J* = 6.8 Hz, 1H), 7.14 (d, *J* = 8.6 Hz, 4H), 7.05 (d, *J* = 8.6 Hz, 2H), 6.87 (d, *J* = 8.6 Hz, 4H), 3.96–3.93 (t, *J* = 6.0 Hz, 4H), 1.80–1.77 (m, 4H), 1.45–1.25 (br, 32H), 0.89–0.88 (t, *J* = 3.2 Hz, 6H). MALDI-TOF MS (*m*/*z*) for $C_{46}H_{60}BN_3O_4S$, Calcd: 761.440; Found, 761.396.

2.3.3. N,N-di(4-octyloxyphenyl)-4-(7-(quinolin-2-yl)benzo[c][1,2,5]thiadiazol-4-yl)benzenamine (TPA-BT-Q, **4**)

A mixture of compound **3** (0.30 g, 0.39 mmol), 2-bromoquinoline (97 mg, 0.47 mmol), K_2CO_3 (6 mL, 2 M) and $Pd(PPh_3)_4$ (20 mg, 0.02 mmol) in toluene (35 mL) and methanol (6 mL) was heated at 80 °C at nitrogen atmosphere for 12 h. After cooled to RT, the mixture was poured into water (100 mL) and extracted with DCM (3 × 30 mL). The combined organic layer was dried over $MgSO_4$ and then concentrated under reduced pressure. The residue was purified by silica gel column chromatography using DCM/petroleum ether (*V*/*V* = 1/2) as eluent to gain red viscous compound **4** (0.24 g, 79.7%). ^{1}H NMR (400 MHz, $CDCl_3$, ppm): 8.75 (d, *J* = 8.2 Hz, 1H), 8.65 (d, *J* = 7.0 Hz, 1H), 8.36 (d, *J* = 8.4 Hz, 1H), 8.23 (d, *J* = 8.0 Hz, 1H), 7.91–7.86 (br, 4H), 7.79–7.75 (t, *J* = 7.2 Hz, 1H), 7.60–7.57 (t, *J* = 6.6 Hz, 1H), 7.15 (d, *J* = 7.6 Hz, 4H), 7.08 (d, *J* = 7.8 Hz, 2H), 6.87 (d, *J* = 7.8 Hz, 4H), 3.96–3.93 (t, *J* = 6.4 Hz, 4H), 1.80–1.78 (m, 4H), 1.47–1.26 (br, 20H), 0.91–0.89 (t, *J* = 3.8 Hz, 6H). MALDI-TOF MS (*m*/*z*) for $C_{49}H_{54}N_4O_2S$, Calcd: 762.397; Found, 762.376.

2.3.4. (TPA-BT-Q)Ptpic (**5**)

(TPA-BT-Q)Ptpic was synthesized by the common method described above for the general synthesis of the platinum complex and obtained as violet black powder in a yield of 43.4%. ^{1}H NMR (400 MHz, $CDCl_3$, ppm): 9.41 (d, *J* = 8.8 Hz, 1H), 9.33 (d, *J* = 8.8 Hz, 1H), 9.17–9.15 (t, *J* = 4.6 Hz, 1H), 8.33 (d, *J* = 8.8 Hz, 1H), 8.22–8.19 (t, *J* = 6.8 Hz, 1H), 8.16–8.13 (t, *J* = 7.4 Hz, 1H), 7.87–7.81 (br, 3H), 7.74–7.72 (t, *J* = 4.0 Hz, 1H), 7.67 (d, *J* = 6.4 Hz, 2H), 7.54–7.51 (t, *J* = 7.4 Hz, 1H), 7.16 (d, *J* = 8.8 Hz, 4H), 7.03 (d, *J* = 7.8 Hz, 2H), 6.88 (d, *J* = 8.8 Hz, 4H), 3.97–3.94 (t, *J* = 6.4 Hz, 4H), 1.81–1.78 (m, 4H), 1.48–1.28 (br, 20H), 0.91–0.88 (t, *J* = 3.4 Hz, 6H). MALDI-TOF MS (*m*/*z*) for $C_{55}H_{57}N_5O_4PtS$, Calcd: 1078.378; Found, 1078.375. Anal. Calc. for $C_{55}H_{57}N_5O_4PtS$: C 61.21, H 5.32, N 6.49, S 2.97% Found: C 61.51, H 5.22, N 6.11, S 2.90%.

2.3.5. 2-phenylquinoline (PQ, **6**)

2-phenylquinoline was synthesized according to the above procedure of compound **4** and obtained as white solid in a yield of 82.4%. ^{1}H NMR (400 MHz, $CDCl_3$, ppm): 8.24 (d, *J* = 8.6 Hz, 1H), 8.19–8.16 (br, 3H), 7.90 (d, *J* = 8.4 Hz, 1H), 7.85 (d, *J* = 8.0 Hz, 1H), 7.75–7.71 (t, *J* = 7.4 Hz, 1H), 7.55–7.52 (br, 3H), 7.47–7.45 (t, *J* = 7.2 Hz, 1H).

2.3.6. PQPtpic (**7**)

PQPtpic was synthesized according to the above general procedure of platinum complex and obtained as an orange powder in a yield of 45.9%. ^{1}H NMR (400 MHz, $CDCl_3$, ppm): 9.47 (d, *J* = 8.8 Hz,

1H), 9.23 (d, J = 5.4 Hz, 1H), 8.33 (d, J = 8.4 Hz, 1H), 8.25 (d, J = 7.4 Hz, 1H), 8.16–8.14 (t, J = 4.2 Hz, 1H), 8.00–7.89 (t, J = 3.4 Hz, 1H), 7.84–7.82 (t, J = 4.4 Hz, 1H), 7.80–7.78 (t, J = 4.0 Hz, 1H), 7.63–7.60 (br, 3H), 7.34–7.26 (t, J = 5.4 Hz, 1H), 7.24 (d, J = 3.4 Hz, 2H). MALDI-TOF MS (m/z) for $C_{21}H_{14}N_2O_2Pt$, Calcd: 521.070; Found, 521.110.

3. Results and discussion

3.1. Synthesis and characterization

Compound **1** was prepared according to the literature procedures [14]. Compound **2**, TPA-BT-Q and PQ were synthesized through Suzuki couplings. The (TPA-BT-Q)Ptpic and PQPtpic were synthesized using the previous method with two-step procedures, which contain a cyclometalation of TPA-BT-Q, PQ and a cleavage of the chloride groups in the corresponding dimers with picolinic acid. The made (TPA-BT-Q)Ptpic and PQPtpic were characterized by ^{1}H NMR, MALDI-TOF mass spectra and element analysis to confirm their well-defined chemical structures.

3.2. Photophysical properties

Fig. 1 shows the normalized UV–vis spectrum of (TPA-BT-Q)Ptpic in dichloromethane (DCM). For comparison, the normalized UV–vis spectra of the TPA-BT-Q free ligand and the parent platinum (II) complex of PQPtpic in DCM were insetted in Fig. 1. Three typical absorption peaks at 314 nm, 371 nm and 540 nm were observed for (TPA-BT-Q)Ptpic. The intense high-lying absorption peak is ascribed to the spin-allowed ligand-central (LC) π–π^* transitions of TPA-BT-Q, the moderate-lying one from 371 nm to 450 nm is mainly attributed to the mixed spin-allowed and spin-forbidden singlet metal-to-ligand charge transfer (^{1}MLCT and ^{3}MLCT) transitions. The intense and broad low-lying one around 540 nm with an extinction coefficient (ε) of 1.5 × 10^5 L mol^{-1} cm^{-1} is assigned to the intramolecular charge transfer (ICT) transition from TPA unit to the BT and PQPtpic chromophores. Compared to the TPA-BT-Q free ligand, (TPA-BT-Q)Ptpic exhibited a significant red-shift low-lying absorption peak (ca. 65 nm), which is due to the additional MLCT transition and enhanced electron acceptor effect of the PQPtpic chromophore. The red-shift low-lying absorption peak implies that (TPA-BT-Q)Ptpic with D–A–A architecture has an extensional conjugated system and more intense ICT effect than the TPA-BT-Q free ligand due to incorporation of the substituent PQPtpic acceptor unit.

The PL spectra of (TPA-BT-Q)Ptpic, TPA-BT-Q and PQtpic in dilute DCM are displayed at RT in Fig. 2. The corresponding data are summarized in Table 1. Under photo-excitation at 390 nm, the parent complex of PQPtpic displayed two intrinsic structured emission peaks at 555 nm and 590 nm, as well as the slightly structureless excimer emission at 705 nm. This inherent emission is attributed to a mixed emission from MLCT and LC state [13a]. However, TPA-BT-Q and (TPA-BT-Q)Ptpic exhibited a wide red and NIR emission profiles with a peak at 580 nm and 760 nm under photo-excitation at 400 nm and 540 nm, respectively. Compared to PQPtpic and TPA-BT-Q, (TPA-BT-Q)Ptpic presented a bathochromic PL spectrum by 170 nm due to the additional D–A and stronger D–A–A interactions, respectively. This indicates that the intramolecular D–A effect is available to make its platinum complexes exhibit red-shifted PL spectra.

3.3. Thermal properties and dispersibility

Thermal properties of (TPA-BT-Q)Ptpic and PQPtpic were characterized by thermal gravimetric analysis (TGA) under a nitrogen atmosphere with a scanning rate of 20 °C min^{-1}. The recorded TGA curves are shown in Fig. S1 (see Supporting Information, SI). The onset decomposition temperatures for 5% weight loss (T_d) were 287 °C and 202 °C for (TPA-BT-Q)Ptpic and PQPtpic, respectively. It indicates that (TPA-BT-Q)Ptpic has higher thermal stability.

To clarify the dispersibility of this platinum complex in the polymer matrix, the (TPA-BT-Q)Ptpic-doped PVK-PBD films at different doping concentrations from 0.5 wt% to 8.0 wt% were made. The surface morphology was recorded by atomic force microscopy (AFM) and is shown in Fig. S2 (see the SI). Roughness value of R_a = 0.287 nm, 0.274 nm, 0.262 nm, 0.264 nm and 0.321 nm were observed at doping concentrations of 0.5 wt%, 1.0 wt %, 2.0 wt%, 4.0 wt% and 8.0 wt%, respectively. This result means that the D–A–A type platinum (II) complexes exhibited a good dispersibility in the PVK-PBD matrix at these given doping concentrations.

3.4. Electrochemical properties

The redox properties of (TPA-BT-Q)Ptpic was characterized by cyclic voltammetry (CV) method using ferrocene as an internal

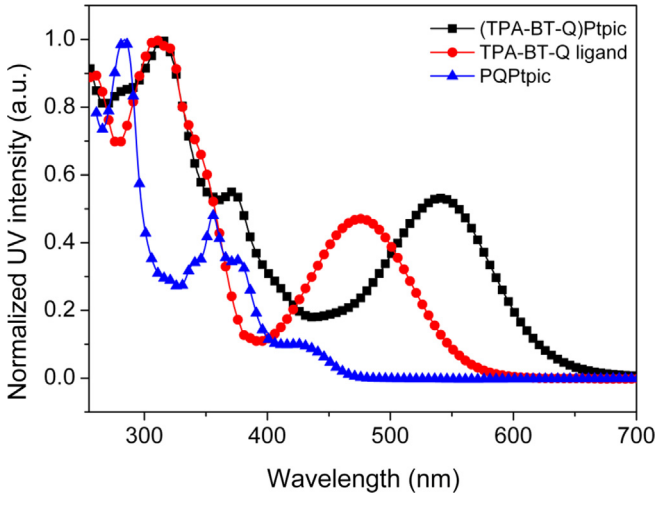

Fig. 1. Normalized UV–vis absorption spectra of TPA-BT-Q, (TPA-BT-Q)Ptpic and PQPtpic in DCM at RT.

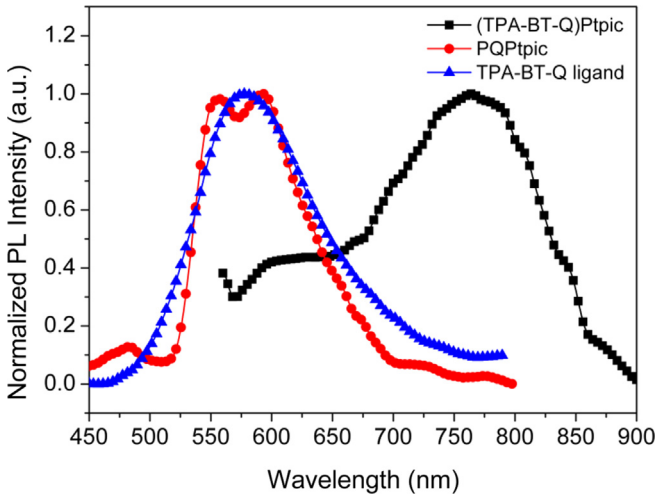

Fig. 2. Normalized PL spectra of TPA-BT-Q, (TPA-BT-Q)Ptpic and PQPtpic in DCM at RT.

Table 1
Photophysical, thermal and electrochemical properties of (TPA-BT-Q)Ptpic.

UV–vis λ/nm[a] (ε_{max}/L mol^{-1} cm^{-1})[b]	PL λ/nm[a]	T_d (°C)[c]	E_{HOMO}/eV[d]	E_{LUMO}/eV[d]
314 (310,526), 371 (144,737), 540 (152,632)	759	287	−4.88	−2.91

[a] Measured in DCM at 298 K at a concentration of 10^{-6} mol L^{-1}.
[b] Molar extinction coefficient.
[c] Temperature at 5% weight loss measured by TGA at a heating rate of 20 °C min^{-1} under nitrogen.
[d] $E_{HOMO} = -(4.40 + E_{ox})$ eV, $E_{LUMO} = -(4.40 + E_{red})$ eV.

standard. An irreversible oxidation wave (E_{ox}) at 0.48 eV and a reversible reduction wave (E_{red}) at −1.49 eV were observed versus Fc/Fc^+ (see supporting information, Fig. S3). According to the reported literature, the oxidation originates from the metal center [13a]. On the basis of E_{ox} and E_{red} values, we can calculate the highest occupied molecular orbital (HOMO) and the lowest unoccupied molecular orbital (LUMO) energy levels (E_{HOMO} and E_{LUMO}) of (TPA-BT-Q)Ptpic based on the empirical formula [15]. The resulting CV data are summarized in Table 1. As the LUMO and HOMO energy levels were −2.20 eV/−5.80 eV for PVK and −2.46 eV/−6.20 eV for PBD [8b], (TPA-BT-Q)Ptpic exhibited a matched energy level with the PVK-PBD blend, which is available for (TPA-BT-Q)Ptpic to play a carrier trap role in the PVK-PBD-hosted PLEDs. In order to conveniently analyze the energy transfer of the guest and host in the PLEDs, the HOMO–LUMO energy levels of all materials used and the device configuration are shown in Fig. S4 (see the SI).

3.5. Electroluminescence properties

Fig. 3 shows the electroluminescent (EL) spectra of the (TPA-BT-Q)Ptpic-doped devices at different dopant concentrations from 0.5 wt% to 8.0 wt%. Three distinct EL peaks at about 429 nm, 630 nm and 764 nm were observed, which are assigned to the PVK-PBD, the (TPA-BT-Q) ligand center (LC) and (TPA-BT-Q)Ptpic emissions compared to the EL spectra of the (TPA-BT-Q)-doped devices in Fig. S5, as well as the corresponding PL spectra of the (TPA-BT-Q)-based DCM solution at an excitation wavelength of 400 nm in Fig. 2 and at different excitation wavelengths in Fig. S6, respectively [16]. At low doping concentration of 0.5 wt%, the EL was dominated by the PVK-PBD. With further increasing dopant concentrations, the PVK-PBD emission was gradually decreased, but the (TPA-BT-Q)-based LC and (TPA-BT-Q)Ptpic emissions were gradually enhanced. When the dopant concentration reached to 2.0 wt%–8.0 wt%, the PVK-PBD emission was quickly quenched and strong NIR emission from (TPA-BT-Q)Ptpic at 764 nm was observed with a shoulder at 630 nm.

The EQE versus current density characteristic of the (TPA-BT-Q)Ptpic-doped devices is shown in Fig. 4 at different dopant concentrations from 0.5 wt% to 8.0 wt%. The corresponding device performance data are summarized in Table 2. The EQEs values were decreased with increasing dopant concentrations. The maximum EQEs of 0.06% at current density of 24.4 mA cm^{-2} and 0.12% at 16.6 mA cm^{-2} were observed in the device at the dopant concentrations of 4.0 wt% and 2.0 wt%, respectively. In order to understand why the roll-off of EQEs was occurred with increasing dopant concentrations, we measured the PL efficiency (Φ_{PL}) of the (TPA-BT-Q)Ptpic-doped PVK-PBD blend films at the different dopant concentrations from 0.5 wt% to 8.0 wt%. The Φ_{PL} values of 8.1%, 4.6% and 1.4% were obtained at the dopant concentrations of 0.5 wt%, 1.0 wt% and 2.0 wt%, respectively. However, the Φ_{PL} values at 4.0 wt% and 8.0 wt% dopant concentrations were not detected by the instrument. It is sure that the Φ_{PL} values are also decreased in the blend films with increasing dopant concentrations. Therefore, the decreasing EQEs with increasing dopant concentrations here is related to the concentration quenching of (TPA-BT-Q)Ptpic. However, the EQE level displayed small roll-off at high current densities, which is favorable for practical applications of OLEDs [17]. We noted that the Pt-metalloporphyrin complexes-based devices usually gave the same phenomenon because this class of planar platinum (II) complexes has relatively long lifetimes which easily result in the dominant exciton decay channel by triplet–triplet annihilation [7,18]. In this case, the (TPA-BT-Q)Ptpic with the D–A–A structure containing the bulky non-planar TPA unit effectively exhibited a suppressed triplet–triplet annihilation at high current densities. The TPA group with alkoxy chain may exert a positive effect for the sluggish roll-off of the EQEs due to reducing π-stacking of dopants and improving dispersibility at the same times.

The current densities (J)–voltage (V) characteristics of the (TPA-BT-Q)Ptpic-doped PVK-PBD devices are shown in Fig. 5 and the EL data are summarized in Table 2. The turn-on voltage of the devices increased from 7.3 V to 14.2 V with increasing doping levels from 0.5 wt% to 8.0 wt%. It indicates that the devices are mainly operated

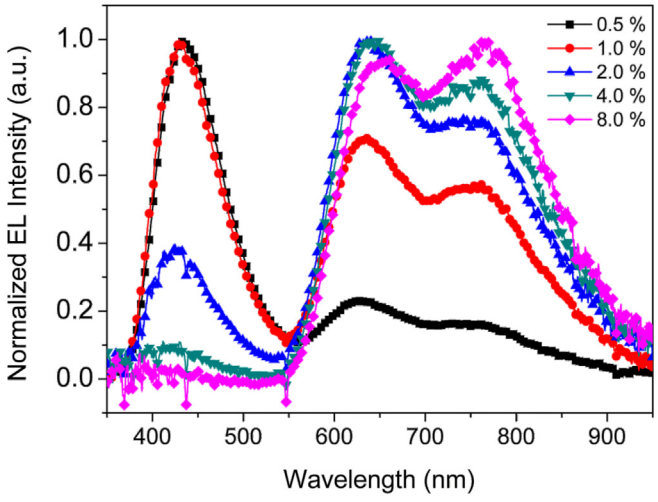

Fig. 3. EL spectra of the (TPA-BT-Q)Ptpic-doped PLEDs at dopant concentrations from 0.5 to 8.0 wt%.

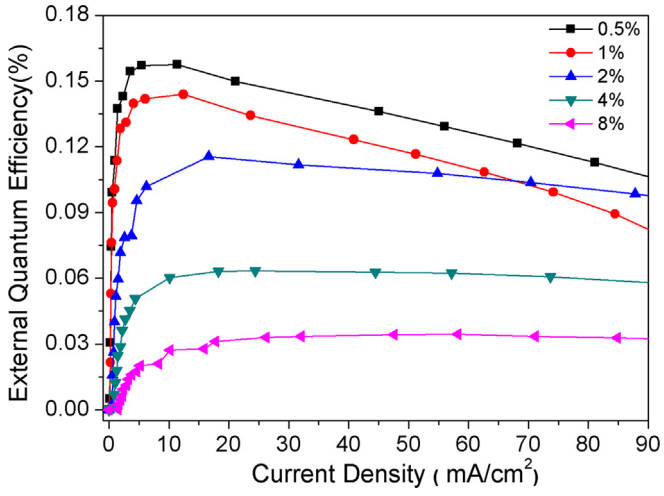

Fig. 4. The external quantum efficiency versus current density characteristics of the (TPA-BT-Q)Ptpic-doped PLEDs.

Table 2
The EL parameters of the (TPA-BT-Q)Ptpic-doped PLEDs.

Dopant (wt%)	0.5	1.0	2.0	4.0	8.0
V_{on} (V)[a]	7.3	8.8	10.7	14.2	14.2
λ_{EL} (nm)[b]	432,625,759	429,633,760	427,637,760	422,637,762	655,766
EQE_{max} (%)[c]	0.16	0.14	0.12	0.06	0.03
J (mA cm^{-2})[d]	11.36	12.41	16.61	24.42	47.62
R (μW cm^{-2})[e]	153	141	112	53	29

[a] V_{on}: turn-on voltage at 1 cd cm^{-2}.
[b] λ_{EL}: the maximum EL emission peak.
[c] EQE_{max}: the maximum external quantum efficiency.
[d] Current density at maximum EQE.
[e] Radiant intensity obtained at an applied current density of 11.7 mA cm^{-2}.

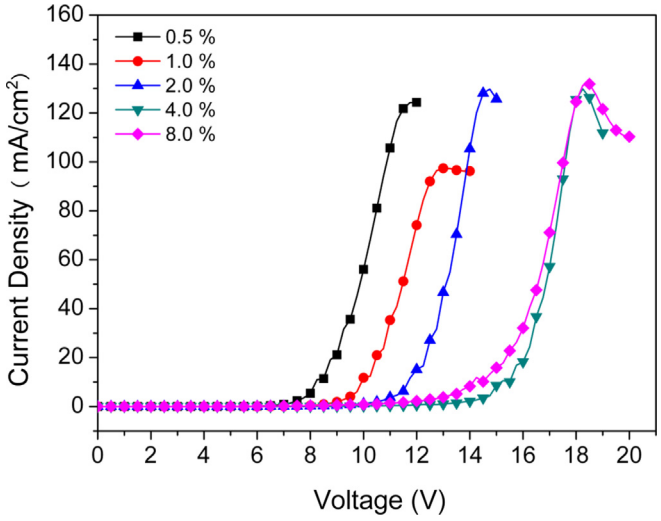

Fig. 5. The current density–voltage (J–V) curves of the (TPA-BT-Q)Ptpic-doped devices at different concentrations from 0.5 to 8.0 wt%.

by the carrier-trapping mechanism based on the identical phenomenon observed previously by Chang et al. [19]. On the other hand, the light outputs of 53 μW cm^{-2} and 112 μW cm^{-2} at 11.7 mA cm^{-2} were obtained in the device at 4.0 wt% and 2.0 wt% doping concentrations, respectively. These radiant emittances are comparable to those levels of the reported metallo-porphyrins.

4. Conclusions

In summary, a novel D–A–A platinum (II) complex of (TPA-BT-Q)Ptpic with NIR emission at 760 nm was obtained. Employing it as a dopant, the NIR-emitting PLEDs showed a suppressed efficiency roll-off with increasing operating current density. The best device performances were presented in the device at 2.0 wt% dopant concentration. The maximum EQE of 0.12% at 16.6 mA cm^{-2} and an irradiance intensity of 112 μW cm^{-2} at 11.7 mA cm^{-2} were observed.

Acknowledgments

This work was supported by financial support from the National Natural Science Foundation of China (51273168, 21202139, 50973093), the Innovation Group in Hunan Natural Science Foundation (12JJ7002), the Scientific Research Fund of Hunan Provincial Education Department (10A119, 11CY023, 10B112), Natural Science Foundation of Hunan (12JJ4019, 11JJ3061), the Scientific Research Fund of Xiangtan University (11QDZ18, 2011XZX08), and the Postgraduate Science Foundation for Innovation in Hunan Province (CX2012B249).

Appendix A. Supplementary data

Supplementary data related to this article can be found at http://dx.doi.org/10.1016/j.dyepig.2014.03.040.

References

[1] (a) Qian G, Wang ZY. Near-infrared organic compounds and emerging applications. Chem Asian J 2010;5:1006–29;
(b) Xiang HF, Cheng JH, Ma XF, Zhou XG, Chruma JC. Near-infrared phosphorescence: materials and applications. Chem Soc Rev 2013;46:6128–85.
[2] (a) Eliseeva SV, Bünzli JCG. Lanthanide luminescence for functional materials and bio-sciences. Chem Soc Rev 2010;39:189–227;
(b) Artizzu F, Mercuri ML, Serpe A, Deplano P. NIR-emissive erbium-quinolinolate complexes. Coord Chem Rev 2011;255:2514–29.
[3] (a) Ellinger S, Graham KR, Shi P, Farley RT, Steckler TT, Brookins RN, et al. Donor–acceptor–donor-based π-conjugated oligomers for nonlinear optics and near-IR emission. Chem Mater 2011;23:3805–17;
(b) Qian G, Dai B, Luo M, Yu DB, Zhan J, Zhang ZQ, et al. Donor–acceptor–donor charge-transfer heteroquinoid-based chromophores: near infrared photoluminescence and electroluminescence. Chem Mater 2008;20:6208–16.
[4] (a) Jiao C, Huang KW, Wu J. Perylene-fused BODIPY dye with near-IR absorption/emission and high photostability. Org Lett 2011;13:632–5;
(b) Ma X, Mao XR, Zhang SW, Huang XB, Cheng YX, Zhu CJ. Nucleation ability of multiwall carbon nanotubes in polypropylene composites. Polym Chem 2013;4:520–7.
[5] (a) Wu XG, Liu Y, Wang YF, Wang L, Tan H, Zhu MX, et al. Highly efficient near-infrared emission from binuclear cyclo-metalated platinum complexes bridged with 5-(4-octyloxyphenyl)-1,3,4-oxadiazole-2-thiol in PLEDs. Org Electron 2012;13:932–7;
(b) Yang CJ, Yi C, Xu M, Wang JH, Liu YZ, Gao XC, et al. Red to near-infrared electrophosphorescence from a platinum complex coordinated with 8-hydroxyquinoline. Appl Phys Lett 2006;89:233506;
(c) Lee TC, Hung JY, Chi Y, Cheng YM, Lee GH, Chou PT, et al. Rational design of charge-neutral, near-infrared-emitting osmium(II) complexes and OLED fabrication. Adv Funct Mater 2009;19:2639–47;
(d) Mori H, Tanaka T, Osuka A. Fused porphyrinoids as promising near-infrared absorbing dyes. J Mater Chem C 2013;1:2500–19;
(e) Xiang HF, Xu ZX, Roy VAL, Yan BP, Chan SC, Che CM, et al. Deep-red to near-infrared electrophosphorescence based on bis(8-hydroxyquinolato) platinum(II) complexes. Appl Phys Lett 2008;92:163305;
(f) Tao R, Qiao J, Zhang GL, Duan L, Wang LD, Qiu Y. Efficient near-infrared-emitting cationic iridium complexes as dopants for OLEDs with small efficiency roll-off. J Phys Chem C 2012;116:11658–64;
(g) Tao R, Qiao J, Zhang GL, Duan L, Chen CC, Wang LD, et al. High-efficiency near-infrared organic light-emitting devices based on an iridium complex with negligible efficiency roll-off. J Mater Chem C 2013;1:6446–54.
[6] Baldo MA, O'Brien DF, You Y, Shoustikov A, Sibley S, Thompson ME, et al. Highly efficient phosphorescent emission from organic electroluminescent devices. Nature 1998;395:151–4.
[7] Borek C, Hanson K, Djurovich PI, Thompson ME, Aznavour K, Bau R, et al. Highly efficient, near-infrared electrophosphorescence from a Pt-metallo-porphyrin complex. Angew Chem Int Ed 2007;46:1109–12.
[8] (a) Shi DY, Wang YF, Liu Y, Zhang ZY, Luo J, He J, et al. Star-shaped trinuclear cyclometalated platinum (II) complexes as single-component emitters in white-emitting PLEDs. Chem Asian J 2012;7:2096–101;
(b) Shigehiro T, Yagi S, Maeda T, Nakazumi H, Fujiwara H, Sakurai Y. Photo- and electroluminescence from 2-(dibenzo[b,d]furan-4-yl)pyridine-based heteroleptic cyclometalated platinum (II) complexes: excimer formation drastically facilitated by an aromatic diketonate ancillary ligand. J Phys Chem C 2013;117:532–42;

(c) Fukagawa H, Shimizu T, Hanashima H, Osada Y, Suzuki M, Fujikake H. Highly efficient and stable red phosphorescent organic light-emitting diodes using platinum complexes. Adv Mater 2012;24:5099–103;
(d) Kui SCF, Hung FF, Lai SL, Yuen MY, Kwok CC, Low KH, et al. Luminescent organoplatinum(II) complexes with functionalized cyclometalated CNC ligands: structures, photophysical properties and material applications. Chem Eur J 2012;18:96–109.

[9] Shimizu M, Kaki R, Takeda Y, Hiyama T, Nagai N, Yamagishi H, et al. 1,4-Bis(diarylamino)-2,5-bis(4-cyanophenylethenyl)benzenes: fluorophores exhibiting efficient red and near-infrared emissions in solid State. Angew Chem Int Ed 2012;51:4095–9.

[10] Qian G, Zhong Z, Luo M, Yu DB, Zhang ZQ, Wang ZY, et al. Simple and efficient near-infrared organic chromophores for light-emitting diodes with single electroluminescent emission above 1000 nm. Adv Mater 2009;21:111–6.

[11] Hu ZY, Wang YF, Shi DY, Tan H, Li XS, Wang L, et al. Highly-efficiency red-emitting platinum(II) complexes containing 4′-diarylamino-1-phenyl-isoquinoline ligands in polymer light-emitting diodes: synthesis, structure, photoelectron and electroluminescence. Dyes Pigments 2010;86:166–73.

[12] (a) Zhang BH, Qin CJ, Ding JQ, Chen L, Xie ZY, Cheng YX, et al. High-performance all-polymer white-light-emitting diodes using polyfluorene containing phosphonate groups as an efficient electron-injection layer. Adv Funct Mater 2010;20:2951–7;
(b) Luo J, Li XZ, Hou Q, Peng JB, Yang W, Cao Y. High-efficiency white-light emission from a single copolymer: fluorescent blue, green, and red chromophores on a conjugated polymer backbone. Adv Mater 2007;19:1113–7;
(c) Zhu WH, Wu YZ, Wang ST, Li WQ, Li X, Chen J, et al. Organic D–A–π–A solar cell sensitizers with improved stability and spectral response. Adv Funct Mater 2011;21:756–63;
(d) Wu YZ, Zhu WH. Organic sensitizers from D–π–A to D–A–π–A: effect of the internal electron-withdrawing units on molecular absorption, energy levels and photovoltaic performances. Chem Soc Rev 2013;42:2039–58.

[13] (a) Brooks J, Babayan Y, Lamansky S, Djurovich PI, Tsyba I, Bau R, et al. Synthesis and characterization of phosphorescent cyclometalated platinum complexes. Inorg Chem 2002;41:3055–66;
(b) Wang YF, Liu Y, Li XS, Qi HR, Zhu MX, Wang L, et al. Novel cyclometalated platinum (II) complex containing alkyl-trifluorene picolinic acid as emitter for single-layer white PLEDs. Org Electron 2010;11:1954–9.

[14] (a) Li JM, Deng XP, Zhang ZY, Wang YF, Liu Y, He KQ, et al. Tuning photovoltaic performance of 9,9-dioctylfluorene-alt-5,7-bis(thiophen-2-yl)-2,3-biphenylthieno[3,4-b]pyrazine copolymeric derivatives by attaching additional donor units in pendant phenyl ring. J Polym Sci Pol Chem 2012;50:4686–94;
(b) Zeng WD, Cao Y, Bai Y, Wang YH, Shi YS, Zhang M, et al. Efficient dye-sensitized solar cells with an organic photosensitizer featuring orderly conjugated ethylenedioxythiophene and dithienosilole blocks. Chem Mater 2010;22:1915–25;
(c) Medina A, Claessens CG, Rahman GMA, Lamsabhi AM, Mó O, Yáñez M, et al. Accelerating charge transfer in a triphenylamine–subphthalocyanine donor–acceptor system. Chem Commun 2008;15:1759–61.

[15] Dou L, Gao J, Richard E, You J, Chen CC, Cha KC, et al. Systematic investigation of benzodithiophene-and diketopyrrolopyrrole-based low-bandgap polymers designed for single junction and tandem polymer solar cells. J Am Chem Soc 2012;134:10071–9.

[16] He Z, Wong W-Y, Yu X, Kwok H-S, Lin Z. Phosphorescent platinum (II) complexes derived from multifunctional chromophores: synthesis, structures, photophysics, and electroluminescence. Inorg Chem 2006;45:10922–37.

[17] (a) Gao ZQ, Mi BX, Tam HL, Cheah KW, Chen CH, Wong MS, et al. High efficiency and small roll-off electrophosphorescence from a new iridium complex with well-matched energy levels. Adv Mater 2008;20:774–8;
(b) Jou JH, Wang YS, Lin CH, Shen SM, Chen PC, Tang MC, et al. Nearly non-roll-off high efficiency fluorescent yellow organic light-emitting diodes. J Mater Chem 2011;21:12613–8.

[18] Sommer JR, Shelton AH, Parthasarathy A, Ghiviriga I, Reynolds JR, Schanze KS. Photophysical properties of near-infrared phosphorescent π-extended platinum porphyrins. Chem Mater 2011;23:5296–304.

[19] Chang SY, Kavitha J, Li SW, Hsu CS, Chi Y, Yeh YS, et al. Platinum(II) complexes with pyridyl azolate-based chelates: synthesis, structural characterization, and tuning of photo- and electrophosphorescence. Inorg Chem 2006;45:137–46.